INDIAN JOURNAL OF SCIENCE AND TECHNOLOGY

RESEARCH ARTICLE

# Analysis of Mechanical Properties on Resistance Spot Welded Dissimilar Thick Dissimilar Joints: Effect of Welding Current

**V Sabarivasan[1]*, P Sivaraj[1], S Malarvizhi[1], V Balasubramanian[1], S Sathiya[2]**

**1** Centre for Materials Joining and Research (CEMAJOR), Department of Manufacturing Engineering, Annamalai University, Annamalai Nagar, Chidambaram, 608002, Tamil Nadu, India
**2** Department of Computer Science and Engineering, Annamalai University, Annamalai Nagar, Chidambaram, 608002, Tamil Nadu, India

OPEN ACCESS

**Received:** 25-10-2024
**Accepted:** 03-01-2025
**Published:** 05-02-2025

**Citation:** Sabarivasan V, Sivaraj P, Malarvizhi S, Balasubramanian V, Sathiya S (2025) Analysis of Mechanical Properties on Resistance Spot Welded Dissimilar Thick Dissimilar Joints: Effect of Welding Current. Indian Journal of Science and Technology 18(3): 177-183. https://doi.org/10.17485/IJST/v18i3.3511

* **Corresponding author**.

vasansabari1996@gmail.com

**Funding:** None

**Competing Interests:** None



Published By Indian Society for Education and Environment (iSee)

**ISSN**
Print: 0974-6846
Electronic: 0974-5645

## Abstract

**Objectives:** To study the influence of welding current on shear fracture strength properties of the resistance spot welded (RSW) dissimilar joints. **Methods:** The study employed the RSW of DP 800 steel and AISI 1040 steel in the context of car chassis applications. In RSW, weld current is considered a variable parameter, while others are constant. The tensile shear fracture test and microhardness analysis performed correlated with base metals. The shear fractured region of the tensile samples was analyzed utilizing scanning electron microscopy (SEM). **Findings:** The maximum lap-tensile shear fracture load (L-TSFL) and cross-tensile shear fracture load (C-TSFL) achieved were 23 MPa and 19 MPa, respectively. The weld interface exhibits a maximum hardness of approximately 570 HV. The results indicate that an increase in weld current enhances the hardness and shear fracture strength of a dissimilar joint up to a certain threshold, beyond which these properties decrease. **Novelty:** The joining of dissimilar metals with dissimilar thicknesses by resistance spot welding is an inevitable demand in the modern automotive industry. These research results are more insightful for fabricating automotive frames with dissimilar materials and variable thickness.

**Keywords:** Dual Phase Steel; Medium Carbon Steel; Microhardness; Resistance Spot Welding; Tensile Shear Fracture Strength

## 1 Introduction

Joining dual-phase steel and medium carbon steel using resistance spot welding has numerous applications, such as body panels and chassis components in automotive industries, aircraft structural components, robust frames and supports in heavy machinery, railcar components, and structural elements in building and infrastructure. Resistance spot welding is the joining of two or more metal sheets by overlapping each other and applying desired heat and pressure at a point through electrical resistance [1,2].

The significant process parameters of resistance spot welding are welding current, welding time, and electrode force. Gomora et al. [3] examined the joining of DP 800 with low-carbon steel using the GMAW process. The joints were evaluated for their mechanical properties, including microhardness, tensile strength, and impact resistance. The welded specimen exhibited a microhardness of approximately 401 HV in the low-carbon steel grain growth zone (GGZ), attributed to a hardened martensitic phase. Rajarajan et al. [4] examined the metallurgical alterations and TSFL characteristics of RSWed AHSS – DP 800. The TSFL measured was 21.70 kN for straight lap joints and 17.65 kN for cross lap joints, with 7% and 9% elongations, respectively. The straight-lap joint exhibited a tensile strength of 22.94% greater than the cross-lap joint. Kedar et al. [5] analyzed the fracture behavior of spot-welded DP600 steel joints. Micro-tensile testing was employed better to understand hardness variations within and around the spot-welded joints. Additionally, the experimental results were compared and correlated with the simulation results of the joints. Gorti et al. [6] recorded the impact of welding current in RSW of dissimilar metals such as IF steel and HSLA steel. It's been observed that with increased welding current, the nugget profile is larger. It was stated that the formation of martensite, acicular, and widmanstätten ferrites of mixed features within the fusion zone was due to a better cooling price and occasional WT of approximately 0.2 sec – 0.6 sec. Additionally, it defined that the HAZ region attaining a temperature above A3 leads to the formation of elongated grains towards the nugget zone. Lei et al. [7] experimented with the RSW of LCS and SS through various welding modern-day and welding times. The weld nugget region and HAZ reported higher microhardness values than the other zones because of martensite formation in those areas. The macro analysis stated that the nugget zone size was higher at the SS facet than the LCS because of SS's lower thermal and electric conductivity. Wang et al. [8] investigated the alterations in mechanical properties and metallurgical characteristics in resistance spot welded chrome and low carbon steel. The most beneficial welding parameters were established through an orthogonal test, resulting in a WC of 12 kA, a weld time of 80 ms, and an electrode pressure of 8 kN. Three weld zones were identified: the nugget area, comprising martensite, austenite, and dendritic structures; the coarse heat-affected zone (HAZ), characterized by pro-eutectoid ferrite and martensite; and the smaller heat-affected zone, containing ferrite and pearlite. The welding current significantly impacts the shearing strength of RSW joints.

Keke et al. [9] conducted experiments to mitigate expulsion by implementing preheating current in the RSW of UHSS. The optimal condition was determined as a preheating current intensity of 5.2kA for 1000 ms by comparing the plastic shell (nugget area) formed under different preheating current intensities. Validated by stimulation results as 90% increasing thickness of plastic shell by applying preheating current and experimentally found that expulsion prevented even heat input 70.6% higher than reference welding schedule (RWS). Ali et al. [10] discussed the evolution of metallurgical changes and mechanical properties in DP1000 steel by verifying its chemical composition. They observed that the weld nugget microstructure comprised prior austenite grains embedded within a martensitic matrix. From this, they concluded that cross-tension strength is a critical factor influencing the fracture toughness properties of the spot-welded joint. The above literature review shows limited experimental research on joining dissimilar materials in resistance spot welding. This investigation intended to join dual-phase steel and medium carbon steel using resistance spot welding not yet explored. Hence, a challenge has been made to join the dual-phase steel (DP 800) with medium carbon steel (AISI 1040) using the RSW process. Also, the impact of welding current on TSFL and the microhardness properties of resistant spot welded joints have also been evaluated.

## 2 Methodology

### 2.1 Materials and Methods

In this observation, 1.7 mm thick cold rolled AHSS DP800 and 1.5 mm thick medium carbon metal AISI 1040 have been selected for joint fabrication. Table 1 and Table 2 present the base metals' chemical composition and mechanical properties. DP 800 metallic (Figure 1 **a**)is composed of ferrite and martensite, exhibiting an average grain size of 6 to 8$\mu$m and 4 to 6 $\mu$m, respectively. AISI 1040 steel (Figure 1 **b**) is present of ferrite and pearlite, exhibiting an average grain size ranging from 10 to 20 $\mu$m and 0.2 to 1 $\mu$m.

**Table 1. Chemical Composition (wt%) of Base Metal**

| Materials | C | Si | Mn | Cr | P | S | Ni | Mo | Ti | Fe |
|---|---|---|---|---|---|---|---|---|---|---|
| DP800 | 0.146 | 0.88 | 1.500 | 0.025 | 0.007 | 0.0036 | 0.027 | 0.0018 | 0.0016 | Bal |
| AISI1040 | 0.43 | 0.26 | 0.68 | - | 0.022 | 0.015 | - | - | - | Bal |

Several trials were conducted in the fabrication of joints to find the suitable parameter range for joining these two dissimilar metals. The constant and varying parameters were selected from trial experiments, presented in Table 3. Base metals were cut into desired dimensions of 75 mm x 25 mm for fabricating lap and cross-lap joints, as shown in Figure 2**a** and Figure 2 **d**. The

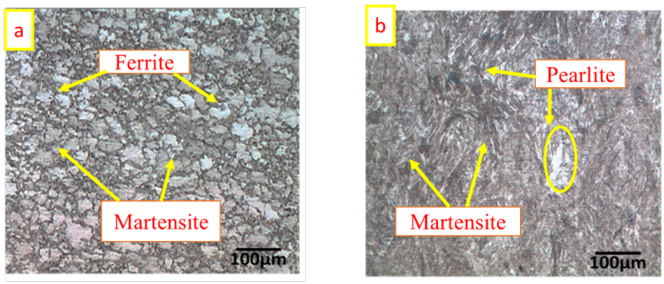


**Fig 1. Microstructure of base metals (a). DP 800 steel (b). AISI 1040 steel**

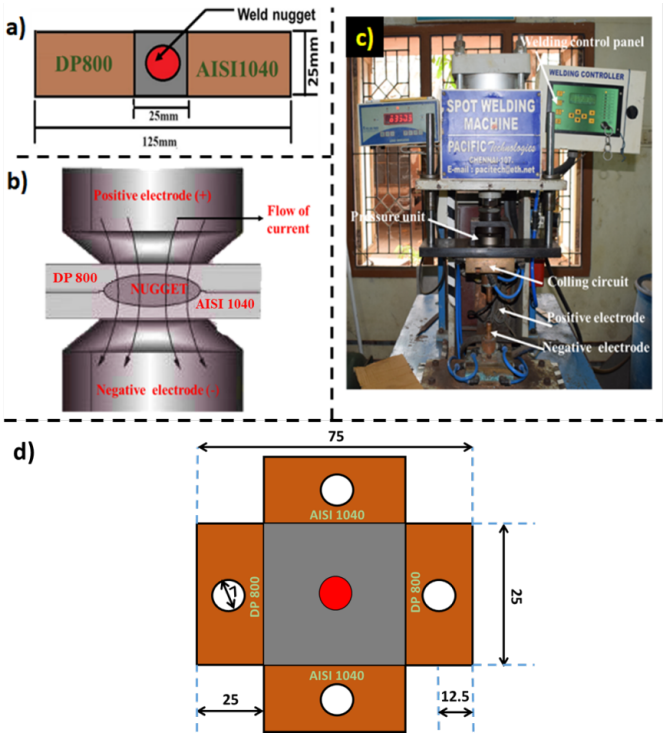


**Fig 2. Experimental setup (a). Lap joint configuration; (b). Welding process; (c). RSW machine; (d). Cross lap joint configuration**

**Table 2. Mechanical Properties of Base Metal**

| Materials | Yield strength (MPa) | Ultimate Tensile Strength (MPa) | Elongation (%) | Hardness (HV) |
|---|---|---|---|---|
| DP800 | 604 | 832 | 26 | 295 |
| AISI1040 | 445 | 612 | 17 | 236 |

schematic diagram of the joining of this dissimilar steel using the RSW process is illustrated in Figure 2 **b**.

The specimens were joined by using Resistance spot welding machine with pedaling mechanism (Model: PACI TECH-ERSW-90 kVA), which is shown in Figure 2**c**. The specimen fabricated in welding current 5kA,5.5 kA, 6kA, 6.5 kA, and 7kA were named W1, W2, W3, W4 and W5. The fabricated lap and cross-lap joints are presented in Figure 3. TSFL tests were conducted as per ASTM – ANSI/SAE/AWS/D8.9 – 13a Standard for both lap joints (L – TSFL) and cross-lap joints (C – TSFL), Universal testing machine (capacity 1000 kN) (Make: FIE-BLUESTAR, INDIA, Model: UNITEK 94100) was employed to carry out the test. The fractured area of L-TSFL and C-TSFL specimens were evaluated using a scanning electron microscope (SEM). Cross-sectioned spot-welded specimens were prepared into metallographic samples for metallurgical evaluation. The samples were mirror polished and etched using Villella's reagent (1g picric acid, 5 ml HCl, and 100 ml ethanol) to obtain macro and microstructures of weld nuggets. A stereo zoom microscope was used to observe the macrostructure of the spot-welded joints.

The microstructure of spot-welded specimens was analyzed through optical microscopy (OM). Microhardness evaluations were conducted using a Vickers hardness trying out machine (Make: SHIMADZU, Japan; model: HMV – T1) to assess the hardness of weld zones and base steel. A load of 0.5 kg was applied for 15 seconds using a diamond indenter on the pass-phase of the welded specimen to acquire correct consequences.

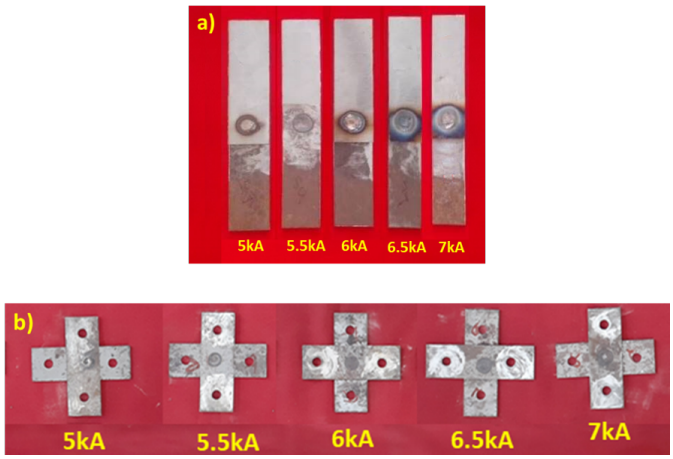


**Fig 3. Fabricated DP 800/AISI 1040 RSW joints in different welding currents (a) Lap joint (b) Cross lap joint**

## 3 Results and Discussion

### 3.1 Tensile Shear Fracture Load

The tensile shear test results of welded specimens are recorded in Table 3. At the same time, Figure 4 displays the fractured L-TSFL and C-TSFL specimens of different DP800/AISI 1040 steel joints as per the Shin et al.[11], when the nugget experiences shear stress, the base metal (BM) and heat-affected zone (HAZ) regions also undergo shear stress in both the thickness and loading directions. Among all the tested specimens (W1, W2, W3, W4, and W5), specimen W3 (6kA) showed the highest L-TSFL and C-TSFL values reaching 23 kN and 19 kN, respectively, with the elongation ranging from 7% to 9%, respectively. These results confirm that increasing the weld current strengthens the joint to some extent (6kA - 23 kN). However, increasing the current results in a decrease in integration. This is because the heat generated by the weld nugget above a current level causes the molten metal to become liquid and the metal to be ejected. This can lead to the loss of essential components in the nugget region, reducing the strength of the joint. According to Sadeghian et al.[12] variations in notch size, tip geometry, the presence and extent of voids or porosities in the nugget zone and heat-affected zone, as well as the indentation depth will affect the shear fracture properties of the joint. Fracture initiation observed in HAZ (heat affected zone) of AISI 1040 MCS side in L–TSFL specimens in tearing failure mode. C–TSFL specimen exhibits pull-out failure mode from weld nugget area. L-TSFL shows 23% higher strength than the C-TSFL, which confirms that the load-carrying capacity of DP800/AISI 1040 dissimilar RSW lap joints is superior to the RSW cross-lap joints.

**Table 3. SFL test results of welded specimens in different welding current**

| Specimens | L-TSFL (kN) | Elongation (%) | C-TSFL (kN) | Elongation (%) |
|---|---|---|---|---|
| W1 | 18 | 3 | 9 | 5 |
| W2 | 23 | 5 | 13 | 7 |
| W3 | 23 | 7 | 19 | 9 |
| W4 | 24 | 6 | 15 | 8 |
| W5 | 19 | 4 | 11 | 6 |

### 3.2 Fractography

The fractured locations of the W3 (6kA) specimen were examined by using SEM, as given in Figure 5. The failure arose along the edge of the nugget zone in both L-TSFL and C-TSFL specimens due to significant plastic deformation of base metal. The dimple sizes in the fractured surface area show the material's deformation and mechanical properties of the weld nugget**.** When comparing the fractured surface area of L–TSFL and C–TSFL, finer dimples and microvoids were observed in L–TSFL. Shear dimples with cleavage facet areas were observed from the fractured area of the C– TSFL specimen. Mishra et al. [13] analyzed the behavior of weld nuggets under cross-tension shear loading and observed that the weld nugget experienced tensile stress and Mode I crack tip opening at its edge. Cleavage facet formation due to carbides in that area leads to crack propagation during the tensile loading [13,14]. The fracture pledges at the HAZ of AISI 1040 side and grows towards base metal in L– TSFL specimen due to the incidence of coarser grains and lower hardness confirmed by observing the vast voids from the fractured surface area.

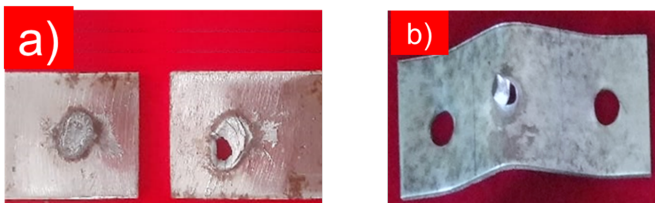


**Fig 4. Fractured DP800/AISI 1040 RSW (W3 – 6kA) joints (a) L-TSFL (Tearing type fracture ; (b) C-TSFL (Pull out type fracture)**

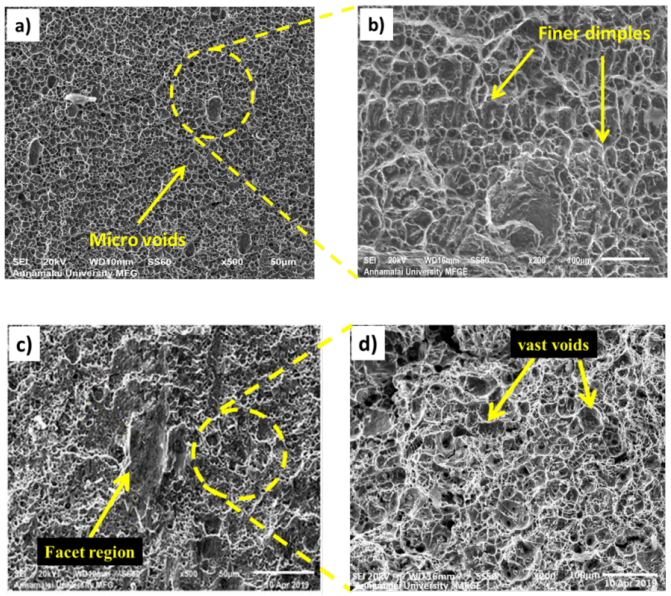


**Fig 5. SEM images of fractured TSFL specimens (W3 – 6kA) in lower and higher magnification (a -b) L – TSFL; (c – d) C –TSFL**

### 3.3 Microhardness

Figure 6 illustrates the Vickers microhardness profile of resistance spot welded specimens subjected to varying welding currents. Hardness variation was noted across all regions, including the weld nugget zone (NZ), fine-grained HAZ (FN - HAZ), and coarse-grained HAZ (CR - HAZ) in the welded joints. The W3 (6kA) specimen demonstrates superior hardness across all zones relative to the other welded specimens (W1, W2, W4, W5). The maximum microhardness value recorded in the nugget zone of W3 was approximately 570 HV. The microhardness value of the weld nugget in specimens W1, W2, W4, and W5 is recorded as 530HV, 550HV, 560HV, and 540HV, respectively. Increased welding current increases weld nugget hardness up to a specific threshold (W3 – 6kA – 570HV); away from this point, additional increases in welding current result in a decrease in hardness. Up to a certain applied welding current, the grain becomes finer in the weld nugget; after that, increased heat at the weld

nugget due to increased welding current leads to grain coarsening, resulting in lower hardness [15,16]. The higher microhardness value at the nugget zone is due to the formation of martensite structure by rapid cooling after welding. The hardness decreases towards HAZ on both sides (DP800 and AISI 1040), which shows the coarsening of grains from the nugget zone to HAZ. Lower hardness was observed in the AISI 1040 CR-HAZ region. The region (CR – HAZ) experiences high temperature, leading to grain coarsening and forming softer phases. Hence, the area becomes weaker than the other zones [17–19]. Therefore, failure occurred in CR- HAZ of AISI 1040 in the RSW DP800/AISI 1040 joints.

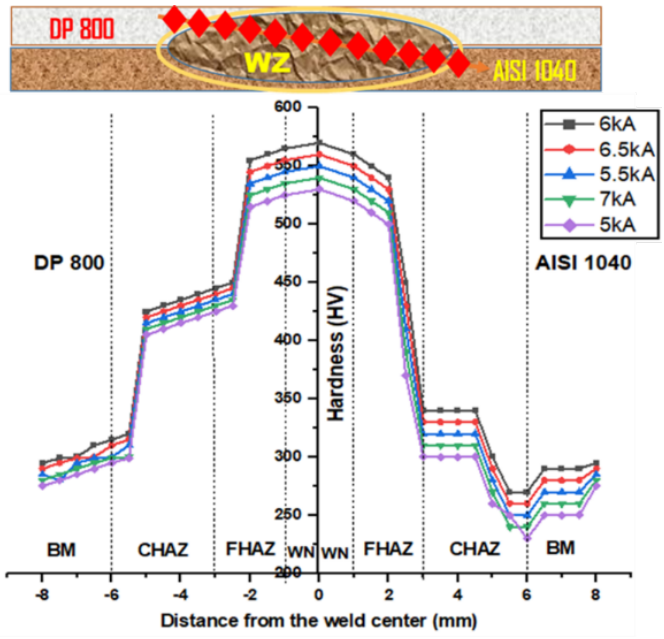


**Fig 6. Microhardness distribution of dissimilar DP800/AISI 1040 RSW joint cross-section**

## 4 Conclusions

This study has investigated the impact of welding current on dissimilar thick steel joints. The mechanical properties were correlated with results, and the following conclusions are made:

- The resistance spot welded DP800/AISI1040 joints fabricated in WC 6kA, electrode pressure 0.4MPa, and WT 4 seconds attain maximum L-TSFL 23kN and C-TSFL 19kN and weld nugget hardness 570 HV.
- The failure attained CR-HAZ of AISI 1040 in a ductile manner due to the formation of coarser ferrite and lower hardness at that zone. The joint efficiency of DP800/AISI 1040 lap joints is higher than the cross-lap joints.
- Increasing the welding current causes higher strength and microhardness value of the weld nugget area up to a certain level; further increasing the welding current tends to lower fracture strength and hardness.
- Further, the fracture behavior and characteristics of resistance spot welded dissimilar joints were studied.

In the future, the fatigue and fracture toughness behavior of dissimilar thickness resistance spot-welded DP800/AISI1040 joints will be investigated.

## References

1) Stavropoulos P, Sabatakakis K. Quality Assurance in Resistance Spot Welding: State of Practice, State of the Art, and Prospects. *Metals*. 2024;14(2). Available from: https://doi.org/10.3390/met14020185.
2) Soomro IA, Pedapati SR, Awang M. A review of advances in resistance spot welding of automotive sheet steels: emerging methods to improve joint mechanical performance. *The International Journal of Advanced Manufacturing Technology*. 2022;118:1335–1366. Available from: https://link.springer.com/article/10.1007/s00170-021-08002-5.
3) Gómora CM, Ambriz RR, García CJ, Ruíz-López I, Jaramillo D. Dissimilar Dual Phase-Low Carbon Steel Joints by the GMAW Process Subjected to Impact Load. *Metals*. 2022;12(3). Available from: https://doi.org/10.3390/met12030404.

4) Rajarajan C, Sivaraj P, Sonar T, Raja S, Mathiazhagan N. Investigation on microstructural features and tensile shear fracture properties of resistance spot welded advanced high strength dual phase steel sheets in lap joint configuration for automotive frame applications. *Journal of the Mechanical Behavior of Materials*. 2022;31(1):52–63. Available from: https://www.degruyter.com/document/doi/10.1515/jmbm-2022-0006/html?lang=en&srsltid=AfmBOoolbo1c2XYYQdd0M2_ES5bv_uZImbKTUvP_WKbyB1DloJApWzMa.
5) Pandya KS, Grolleau V, Roth CC, Mohr D. Fracture response of resistance spot welded dual phase steel sheets: Experiments and modeling. *International Journal of Mechanical Sciences*. 2020;187. Available from: https://doi.org/10.1016/j.ijmecsci.2020.105869.
6) Janardhan G, Mukhopadhyay G, Kishore K, Dutta K. Resistance Spot Welding of Dissimilar Interstitial-Free and High-Strength Low-Alloy Steels. *Journal of Materials Engineering and Performance*. 2020;29(5):3383–3394. Available from: https://link.springer.com/article/10.1007/s11665-020-04857-z.
7) Chen L, Zhang Y, Xue X, Wang B, Yang J, Zhang Z, et al. Investigation on shearing strength of resistance spot-welded joints of dissimilar steel plates with varying welding current and time. *Journal of Materials Research and Technology*. 2022;16:1021–1028. Available from: https://doi.org/10.1016/j.jmrt.2021.12.079.
8) Wang B, Qiu F, Chen L, Zhou Q, Dong B, Yang H, et al. Microstructure and shearing strength of stainless steel/low carbon steel joints produced by resistance spot welding. *Journal of Materials Research and Technology*. 2022;20:2668–2679. Available from: https://doi.org/10.1016/j.jmrt.2022.08.041.
9) Yang K, El-Sari B, Olfert V, Wang Z, Biegler M, Rethmeier M, et al. Expulsion prevention in resistance spot welding of dissimilar joints with ultra-high strength steel: An analysis of the mechanism and effect of preheating current. *Journal of Manufacturing Processes*. 2024;124:489–502. Available from: https://doi.org/10.1016/j.jmapro.2024.06.034.
10) Chabok A, Van Der Aa E, Pei Y. A study on the effect of chemical composition on the microstructural characteristics and mechanical performance of DP1000 resistance spot welds. *Materials science and Engineering: A*. 2020;788. Available from: https://doi.org/10.1016/j.msea.2020.139501.
11) Shin S, Park DJ, Yu J, Rhee S. Resistance Spot Welding of Aluminum Alloy and Carbon Steel with Spooling Process Tapes. *Metals*. 2019;9(4). Available from: https://doi.org/10.3390/met9040410.
12) Sadeghian B, Taherizadeh A, Salehi T, Sadeghi B, Cavaliere P. Simulation and Microstructure Prediction of Resistance Spot Welding of Stainless Steel to Carbon Steel. *Metals*. 2022;12(11). Available from: https://doi.org/10.3390/met12111898.
13) Mishra D, Rajanikanth K, Shunmugasundaram M, Kumar AP, Maneiah D. Dissimilar resistance spot welding of mild steel and stainless steel metal sheets for optimum weld nugget size. *Materials Today: Proceedings*. 2021;46:919–924. Available from: https://doi.org/10.1016/j.matpr.2021.01.067.
14) Yu J, Zhang H, Wang B, Gao C, Sun Z, He P. Dissimilar metal joining of Q235 mild steel to Ti6Al4V via resistance spot welding with Ni-Cu interlayer. *Journal of Materials Research and Technology*. 2021;15:4086–4101. Available from: https://doi.org/10.1016/j.jmrt.2021.10.039.
15) Rajarajan C, Sivaraj P, Sonar T, Raja S, Mathiazhagan N. Resistance spot welding of advanced high strength steel for fabrication of thin-walled automotive structural frames. *Forces in Mechanics*. 2022;7. Available from: https://doi.org/10.1016/j.finmec.2022.100084.
16) Prabhakaran M, Duraisamy J, Shanmugam NS, Kannan AR, Varatharajalu M. Weld Strength and Microstructure Analysis on Resistance Spot Welding of Austenitic AISI 347 Stainless Steel and Duplex AISI 2205 Stainless Steel. *Transactions of the Indian Institute of Metals*. 2023;76:925–936. Available from: https://link.springer.com/article/10.1007/s12666-022-02789-x.
17) Prabhakaran M, Jeyasimman D, Varatharajulu M. Investigation of the failure mechanism of dissimilar resistance spot welding of steels. *Emerging Materials Research*. 2023;12(2):220–228. Available from: https://doi.org/10.1680/jemmr.22.00224.
18) Szwajka K, Zielińska-Szwajka J, Szewczyk M, Mezher MT, Trzepieciński T. Analysis of the Microstructure and Mechanical Performance of Resistance Spot-Welding of Ti6Al4V to DP600 Steel Using Copper/Gold Cold-Sprayed Interlayers. *Materials*. 2024;17(13). Available from: https://www.mdpi.com/1996-1944/17/13/3251.
19) Soomro IA, Pedapati SR, Awang M. Double Pulse Resistance Spot Welding of Dual Phase Steel: Parametric Study on Microstructure, Failure Mode and Low Dynamic Tensile Shear Properties. *Materials*. 2021;14(4). Available from: https://doi.org/10.3390/ma14040802.